Austenite Formation and Decomposition *Edited by E. Buddy Damm and Matthew J. Merwin*
The Iron & Steel Society (ISS) and TMS (The Minerals, Metals & Materials Society), 2003

QUENCHING AND PARTITIONING: A FUNDAMENTALLY NEW PROCESS TO CREATE HIGH STRENGTH TRIP SHEET MICROSTRUCTURES

J.G. Speer,[1] A.M. Streicher,[1] D.K. Matlock,[1] F. Rizzo,[2] and G. Krauss[1]

[1]Advanced Steel Processing and Products Research Center;
Colorado School of Mines; Golden, CO 80401, USA

[2]Department of Materials Science and Metallurgy;
Pontifícia Universidad Católica-Rio de Janeiro; RJ 22453-900, Brazil

Abstract

This paper reviews the implications of a model developed recently to understand and predict the potential extent of carbon partitioning that may occur between as-quenched (carbon supersaturated) martensite, and retained austenite. In the absence of carbide formation, this "constrained paraequilibrium" (or CPE) condition can be calculated based on straightforward thermodynamic and matter balance constraints. Austenite can be highly carbon enriched at constrained paraequilibrium due to rejection from carbon-supersaturated martensite, and the CPE austenite composition can be reasonably approximated by assuming that the total carbon content in the steel is partitioned into the austenite. A new processing concept for production of austenite-containing "TRIP" sheet steels is described, along with a methodology for designing alloys and thermal processing parameters to achieve controlled amounts of retained austenite in the microstructure. The new process is referred to as quenching and partitioning ("Q&P") to distinguish it from conventional quenching and tempering of martensite, which has the objectives of carbide formation and improved toughness, rather than carbon enrichment of retained austenite. Since the CPE partitioning concept assumes that carbide precipitation is absent, suppression of transition carbide formation during partitioning is important, although alloying effects on transition carbide formation are not yet fully clear. Initial experimental verification of the Q&P processing response of a 0.19C, 1.46Mn, 1.96Al sheet steel is presented, and x-ray diffraction data show the presence of substantial amounts of carbon-enriched austenite under different partitioning time/temperature conditions. The experimental results support the general concept of CPE partitioning between martensite and retained austenite, and some further research needs are identified to define more clearly the operative microstructure evolution mechanisms.

Introduction

High strength sheet steels containing significant fractions of retained austenite have been developed in recent years, and are the subject of growing commercial interest. Carbon-enriched metastable retained austenite is considered beneficial because the TRIP phenomenon during deformation can contribute to formability and energy absorption. These steels are typically produced by intercritical annealing, followed by cooling and transforming at a lower temperature, leading to a microstructure of equiaxed (intercritical) ferrite and "carbide-free

bainite" that consists of bainitic ferrite laths with interlath retained austenite. (Alloying additions such as Si or Al are made to suppress cementite formation that usually accompanies bainite formation [1].) Recently, an alternative processing concept has been developed for the production of austenite-containing steels, based on a new understanding of carbon partitioning hypothesized between martensite and retained austenite, whereby metastable "constrained paraequilibrium" (or CPE) is achieved when carbide formation is suppressed by appropriate alloying [2,3]. This paper 1) reviews the CPE carbon partitioning concept, 2) considers important factors related to suppression of carbide formation, and 3) presents the first experimental results applying the associated new processing concepts to a low-carbon TRIP sheet steel composition.

Review of the CPE Partitioning Concept

Carbon partitioning between martensite and retained austenite is usually ignored, because the temperature is usually too low for substantial amounts of carbon diffusion to occur after quenching, and because carbon supersaturation in martensite is usually eliminated by a different mechanism, viz. carbide precipitation during tempering. Consequently, the thermodynamics of carbon partitioning between martensite and retained austenite has not been developed fully. Recently, a model has been developed to address carbon partitioning from as-quenched martensite into austenite, under conditions where competing reactions such as bainite, cementite or transition carbide precipitation are suppressed [2]. The model predicts the "endpoint" of partitioning, when martensite (i.e. ferrite) is in metastable equilibrium with austenite.

Metastable equilibrium between austenite and ferrite is not a new concept [4], and orthoequilibrium and paraequilibrium concepts are well understood at sub-critical temperatures for conditions where partitioning of slow-moving substitutional elements is either complete or absent, respectively. It must be recognized, however, that the approach to ortho- or paraequilibrium necessarily involves interface migration to adjust the phase fractions appropriately, and thus requires short range movements of iron and substitutional atoms, even when long-range substitutional diffusion is precluded as in the paraequilibrium case. When the position of the martensite/austenite interface is effectively *constrained*, as we consider to apply for carbon partitioning between martensite and retained austenite at relatively low temperatures, then even short-range diffusional movements of iron and substitutionals are precluded, and it is not possible for a ferrite/austenite mixture to reach orthoequilibrium in the Fe-C system (or paraequilibrium in multicomponent alloy systems). The metastable α/γ equilibrium in the case of an immobile or constrained interface, is therefore termed "constrained paraequilibrium" or CPE.

Constrained paraequilibrium is essentially defined by one thermodynamic requirement, and one key matter balance constraint. First, carbon diffusion is completed under constrained paraequilibrium conditions when the chemical potential of carbon is equal in the ferrite and austenite. Ignoring effects of alloying on carbon activity, this requirement may be represented using results of Lobo and Geiger [5,6] for the Fe-C binary system as follows:

$$X_C^{\gamma} = X_C^{\alpha} \cdot e^{\frac{76{,}789 - 43.8T - (169{,}105 - 120.4T)X_C^{\gamma}}{RT}} \quad (1)$$

where X_C^{α} and X_C^{γ} represent the mole fractions of carbon in ferrite and austenite. The relevant thermodynamics are embedded in equation #1. This thermodynamic condition may be understood by comparing the schematic Gibbs molar free energy vs. composition diagram in

Figure 1a representing metastable orthoequilibrium in the Fe-C system, with constrained paraequilibrium in Figure 1b.

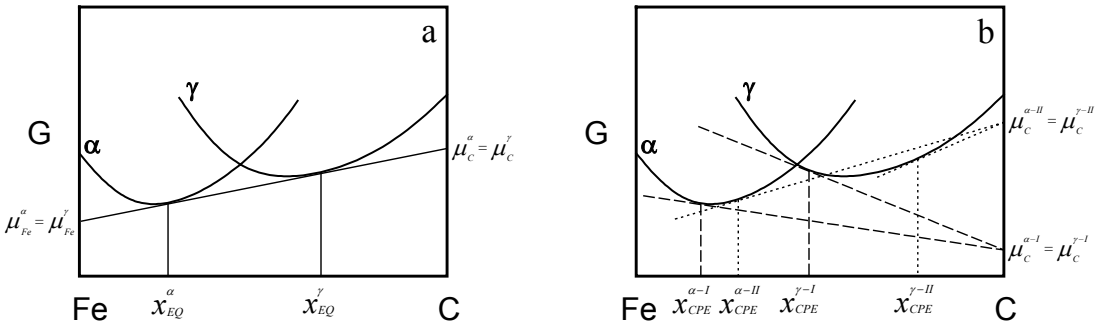

Figure 1. Schematic molar Gibbs free energy vs. composition diagrams illustrating metastable equilibrium at a particular temperature between ferrite and austenite in the Fe-C binary system. a) orthoequilibrium (EQ), and b) two possible constrained paraequilibrium conditions (I and II).

In orthoequilibrium (or paraequilibrium in higher order alloys), there are unique ferrite and austenite compositions (X_{EQ}^{α} and X_{EQ}^{γ}) satisfying the common tangent construction whereby the chemical potentials of both carbon and iron are equal in both phases ($\mu_C^{\alpha} = \mu_C^{\gamma}$ and $\mu_{Fe}^{\alpha} = \mu_{Fe}^{\gamma}$). In constrained paraequilibrium, the thermodynamic condition that the chemical potential of carbon is equal in both phases requires only that the tangents to the ferrite and austenite free energy curves must intersect the carbon axis at a single point. This condition can be satisfied by an infinite set of phase compositions [7], and examples of two such conditions are given in Figure 1b, one which is associated with phase compositions ($X_{CPE}^{\alpha-II}$ and $X_{CPE}^{\gamma-II}$) having a higher carbon concentration than the orthoequilibrium phase compositions, and one associated with phase compostions ($X_{CPE}^{\alpha-I}$ and $X_{CPE}^{\gamma-I}$) having lower carbon levels than orthoequilibrium. The actual CPE phase compositions must also satisfy the unique matter balance constraint associated with the stationary α/γ interface. This second constraint requires that the number of iron (and substitutional) atoms is conserved in each phase during carbon partitioning. Mathematically, this matter balance for iron may be represented by:

$$f_{CPE}^{\gamma}(1 - X_{C_{CPE}}^{\gamma}) = f_i^{\gamma}(1 - X_C^{alloy}) \tag{2}$$

where X_C^{alloy} is the overall carbon content of the steel (in atom fraction, recognizing also that in Fe-C binary alloys, $1 - X_C = X_{Fe}$), f_i^{γ} is the mole fraction of retained austenite before partitioning begins, and f_{CPE}^{γ} and $X_{C_{CPE}}^{\gamma}$ represent the austenite amount and carbon concentration, respectively, at constrained paraequilibrium when carbon partitioning is complete. (A small change in austenite fraction is consistent with transfer of carbon atoms across the interface.) Constrained paraequilibrium is achieved when equations #1-2 above, and #3-4 below are satisfied, where the mass balance for carbon is represented by:

$$f_{CPE}^{\alpha} X_{C_{CPE}}^{\alpha} + f_{CPE}^{\gamma} X_{C_{CPE}}^{\gamma} = X_C^{alloy} \tag{3}$$

and the relationship between the phase fractions of α and γ is simply:

$$f_{CPE}^{\alpha} + f_{CPE}^{\gamma} = 1. \tag{4}$$

Example CPE calculations have been reported in a recent publication [2], where it was shown that most of the carbon in the steel is expected to partition to the austenite, and quite high levels

of carbon enrichment are possible. The dependence of the metastable CPE condition on alloy carbon content, temperature, and the as-quenched austenite and martensite phase fractions was also illustrated. While the detailed calculations are not difficult, *the austenite composition at constrained paraequilibrium can be closely approximated by assuming that virtually all of the carbon in the martensite partitions to the austenite*, and applying the appropriate carbon matter balance based on the amount of retained austenite present after quenching. An implication of these carbon balance considerations is that there is a tradeoff between the amount of austenite present and the degree of carbon enrichment that is possible in a given steel, although higher overall carbon levels in the steel provide the potential for greater amounts of higher carbon austenite.

The results of the constrained paraequilibrium model suggested a new process, whereby austenite is formed at high temperature (either by full austenitization or intercritical heat treatment), followed by cooling to a temperature carefully selected (between M_s and M_f) to control the fractions of martensite and retained austenite, and finally by a thermal treatment that accomplishes the desired carbon partitioning to enrich the austenite with carbon and stabilize some (or all) of it to room temperature. This process sequence and the corresponding microstructural changes are illustrated schematically in Figure 2 [3]. The process assumes that carbon supersaturation is relieved by diffusion into retained austenite, and is referred to as quenching and partitioning, or Q&P, to distinguish it mechanistically from conventional quenching and tempering (Q&T) of martensite, where carbide precipitation and decomposition of retained austenite (to ferrite plus cementite) are typical.

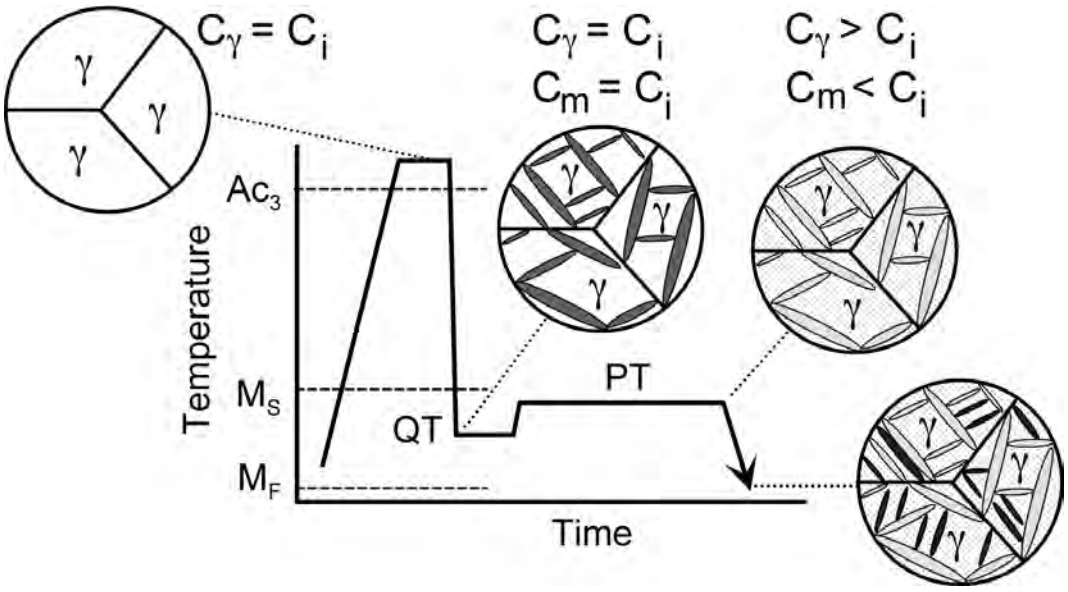

Figure 2. Schematic illustration of the Q&P process for producing of austenite-containing microstructures. C_i, C_γ, C_m represent the carbon contents of the initial alloy, austenite, and martensite, respectively. QT and PT are the quenching and partitioning temperatures.

The example in Figure 2 indicates an initial full austenitization step, although intercritical annealing is also envisioned for sheet products, where a smaller initial fraction of austenite is present with a higher initial carbon content. Initial investigation of the Q&P processing concept verified the presence of significant amounts of carbon enriched austenite in a 0.35C, 1.3Mn, 0.74Si microalloyed bar steel, despite the apparent formation of some transition carbides during the partitioning treatment [3].

The quenching and partitioning heat treatment was envisioned to have application to high-strength austenite containing TRIP sheet steel products, replacing an isothermal bainitic heat treatment of low-carbon steels containing substantial additions of Si, Al, or P to suppress carbide formation. Some perceived advantages of Q&P include the potential for greater carbon enrichment of austenite, decoupling of the (bainitic) ferrite growth kinetics from the carbon partitioning process, and increasing strength via formation of substantial quantities of lath martensite in the microstructure. Other opportunities may exist to employ retained austenite through Q&P processing of higher strength bar steels or even austempered ductile cast iron. Finally, it was suggested that a specific CPE phase composition (where the austenite composition approximates T_o) might even represent a viable steady state boundary condition at the α/γ interface during bainitic ferrite growth, providing a model for the bainite transformation mechanism that is both "fully" diffusional and "fully" martensitic [2].

Suppression of Carbide Precipitation

The absence of carbide formation is a fundamental element of the constrained paraequilibrium model, since the existence of metastable equilibrium between ferrite and austenite is precluded if the more stable ferrite plus iron carbide equilibrium can be achieved. Any carbide formation effectively "consumes" carbon, since it is no longer available to enrich the austenite. Thus, it will be necessary to understand and control carbide precipitation processes that may occur during any partitioning treatments associated with the Q&P process.

It is well known in the bainite transformation literature that cementite formation can be eliminated or suppressed through additions of silicon [1,8], and also that aluminum and even phosphorus can have this effect [9]. Such elements thus play a critical enabling role in the Q&P process. It is also well known in the martensite tempering literature that silicon suppresses cementite formation, or delays the transition from early-stage tempering (where ε or η carbides are present), to later-stage tempering (where θ-Fe_3C is present) [10,11,12]. In martensite, fine transition carbides are usually not considered detrimental, whereas cementite can be of more concern. Thus, the greater emphasis has been on understanding when transition carbides are replaced by cementite formation [12,13], rather than on the *initiation* of transition carbide precipitation. For Q&P processing, however, any transition carbide precipitation diminishes the potential for carbon enrichment of austenite, and so the onset of transition carbide formation is also very important (including compositional effects and sensitivity to processing temperatures/times).

In martensite tempering, transition carbide precipitation is often considered to be complete while the carbon supersaturation in the martensite matrix remains substantial, with a carbon content on the order of 0.25% [10,11]. By implication, it may be concluded that transition carbide formation demands quite high supersaturation, and is therefore more likely under conditions of low temperature and high solute carbon. (The activation energy for transition carbide formation increases with increasing solute carbon, however, due to increased interstitial site occupancy and lattice distortion [11]; consequently, there are also some factors mitigating precipitation at higher supersaturation.) While silicon has low solubility in cementite and clearly delays cementite precipitation during tempering, the alloying effects on transition carbide precipitation are less clear. Silicon is believed to be soluble in transition carbides, and a variety of solute additions are reported to increase the stability of carbon supersaturated martensite [11,12].

Precipitation of transition carbides within retained austenite during martensite tempering has not been documented. Since the chemical potential of carbon is much higher in as-quenched

martensite than in the retained austenite, it is reasonable to conclude that carbide nucleation would be more likely in bcc ferrite than in austenite. This behavior is consistent with results of Barbé *et al*. on a 1.87C, 1.53Mn, 1.57Si steel quenched in liquid N_2 to provide a martensite/austenite mixture [14]. Upon tempering at temperatures of 170 and 300°C, they report η-carbides in the martensite, but not austenite. The α/γ interface is also a favored site for carbide formation.

While the martensite literature does not provide specific guidance for controlling transition carbide formation during partitioning in Si or Al-added steels, the austempered ductile iron (ADI) literature is also relevant in this regard. Heat treating of austempered ductile iron involves formation of hypereutectoid austenite, followed by austempering at temperatures in the range of about 300-400°C to create "ausferrite," which is essentially ferrite plates in a matrix of carbon-enriched retained austenite, where the austenite fraction can be quite high and the carbon concentration in the austenite is on the order of 2%. The microstructure is similar to "carbide-free" ferrite/austenite mixtures that typically form from hypoeutectoid austenite, as discussed in the bainite literature. Silicon often plays a key role in austenite retention in both instances, through its delaying effect on carbide precipitation. The carbides that form during austempering are usually reported to be transition carbides, followed eventually by cementite at longer treatment times [15]. The presence of stable austenite is reported to be enhanced by alloying with silicon, along with other elements (e.g. Mn, Mo, and Ni) [15]. Aluminum can also be substituted for silicon in ADI. In one study, η carbides are reported in the ferrite in both Si and Al grades after a few hours of austempering at 350 or 400°C, with χ–carbides present later at the α/γ interface, and ε is reported at lower temperature [16]. (These processing times are longer than are usually encountered in sheet steel processing, however.) Similarly, Rouns and Rudman indicate that transition carbide formation within the ferrite appears to consume carbon in ADI at low austempering temperatures, whereas the austenite is more fully enriched at higher austempering temperatures [15]. This observation is also consistent with the results of Le Houillier *et al*. on isothermally transformed bainite in a Si-containing 9262 steel, which indicate that largely all of the carbon is partitioned to the austenite in the carbide-free "upper bainite" reaction at 400°C, while the austenite contains substantially less of the available carbon after transformation to lower bainite at 275°C [17].

The levels of austenite carbon enrichment reported in optimally processed Si or Al-containing bainitic steels and austempered ductile iron certainly confirm that transition carbide and cementite formation can be suppressed effectively. The bainite and ADI experiences also suggest that transition carbides might be less likely at processing temperatures higher than are typical of low-temperature martensite tempering, although it is not fully clear how alloying effects are coupled with temperature effects that influence precipitation behavior of each carbide species. That is, transition carbides may simply be inhibited by elevated temperature processing (because of the greater solubility of non-equilibrium phases), or the kinetics may specifically be suppressed at these temperatures by Si or Al additions. An implication for Q&P processing is that partitioning temperatures around 400°C might be preferred relative to much lower temperatures, based on the greater likelihood of transition carbide precipitation at much lower temperatures. However, in the Q&P process, high carbon supersaturation of the martensite prior to partitioning could conceivably drive transition carbide formation to a greater extent than would be possible during bainite growth at the same temperature, since the bainitic ferrite would have a much lower carbon content. The extent to which carbide formation is suppressed will be a critical factor influencing the microstructures that are achievable using the Q&P process, and further studies are needed to establish more clearly the influences of alloying and processing on the carbide precipitation kinetics in these steels.

Sheet Steel Q&P Process Design

A Q&P process design methodology was outlined in a recent publication [3], which is expanded here and modified to include intercritically annealed starting microstructures. This model will be applied to the TRIP sheet steel composition selected for this investigation, shown in Table I. (This high-Al steel is a duplicate heat having a chemical composition similar to the material used in a recent characterization of microstructure evolution after intercritical annealing and isothermal transormation [9,18].)

Table I. Chemical Composition of Experimental High-Al TRIP Sheet Steel

C	Al	Mn	Si	P	N	Cr	S
0.19	1.96	1.46	0.022	0.01	0.0018	0.08	0.002

The intercritical annealing temperature controls the initial microstructure, and TRIP sheet steels typically contain about 50% intercritical austenite, with 50% equiaxed ferrite that remains in the final microstructure. Such a condition provides a useful starting condition to compare Q&P sheet processing with conventional isothermal bainitic treatment. The initial carbon concentration of the austenite is also controlled by the intercritical annealing temperature, and may be estimated assuming that nearly all of the carbon in the steel is contained in the austenite, since the carbon solubility in ferrite is very low. For example, in the steel composition of interest here (containing 0.19%C), if the intercritical microstructure contained 50% austenite, then the carbon concentration of the austenite would be approximately 0.38%C. The quench temperature (QT in Figure 2) controls the martensite fraction according, for example, to the Koistinen-Marburger [10] relationship:

$$f_m = 1 - e^{-1.1 \times 10^{-2}(M_s - QT)} \quad (5)$$

where f_m is the fraction of austenite that transforms to martensite upon quenching to a temperature QT below the M_s temperature. M_s can be predicted for the applicable austenite composition using empirical relations such as [19]:

$$M_s(^oC) = 539 - 423C - 30.4Mn - 7.5Si + 30Al \quad (6)$$

In austenite containing 0.19C, 1.46Mn, and 1.96Al, for example, the M_s temperature is estimated to be approximately 473^{o}C, and the amounts of martensite and retained austenite can be predicted at different quench temperatures using the Koistinen and Marburger relationship above.

Finally, a partitioning treatment is used to transport carbon from martensite to retained austenite. The preferred times and temperatures are not yet clearly established for the partitioning treatment, and are explored as part of this work. As mentioned previously, if carbide precipitation is avoided, then the level of carbon enrichment of the austenite when partitioning is completed (the CPE condition) can be approximated by assuming that virtually all of the carbon partitions to the austenite at the partitioning temperatures of interest in this work. Calculations using these process design concepts were made to provide guidelines to explore processing options that could lead to particular end microstructures of interest. Example results are shown in Table II for the steel used in this investigation, where the fraction of intercritical ferrite and a desired fraction of austenite (at the quench temperature) are inputs to the calculation, and the required quench temperature and the expected carbon concentration of the austenite after partitioning are outputs.

Table II. Estimation of Quench Temperatures to Achieve Controlled Austenite Fractions in Experimental Steel Processed With Different Intercritical Microstructures

Intercritical Microstructure		M_s of Initial Austenite (^oC)	Carbon in Initial Austenite (wt. pct.)	Quench Temperature to Achieve Desired Austenite Fraction	Microstructure at Quench Temperature			Carbon in Austenite After Partitioning (wt. pct.)
% γ	% α				% γ	% α	% M	
100	0	473	0.19	201	5	0	95	3.8
100	0	473	0.19	264	10	0	90	1.9
75	25	448	0.25	265	10	25	65	1.9
50	50	393	0.38	247	10	50	40	1.9
25	75	232	0.76	149	10	75	15	1.9
100	0	473	0.19	301	15	0	85	1.27
75	25	448	0.25	302	15	25	60	1.27
50	50	393	0.38	284	15	50	35	1.27
25	75	232	0.76	186	15	75	10	1.27
100	0	473	0.19	327	20	0	80	0.95
75	25	448	0.25	328	20	25	55	0.95
50	50	393	0.38	310	20	50	30	0.95
25	75	232	0.76	212	20	75	5	0.95

The results in Table II highlight possible quench temperatures that could be employed to achieve variations in retained austenite (at the quench temperature) from 5 to 20%, under conditions where the fraction of intercritical ferrite varies between 0 and 75%. For the experimental work reported here, an intercritical microstructure containing 50% α and 50% γ was selected, along with an aim austenite fraction of 15% at the quench temperature. The estimated M_s temperature for intercritical austenite (of this amount) is about 393^oC. A quench temperature of 284^oC was therefore identified for initial experimentation, to explore the response to subsequent partitioning treatments.

The process design approach was also developed in a more generic form for general application. Calculations in Figure 3 show the combinations of austenite fraction and austenite composition (carbon content), that would be expected in steels of three different carbon levels, after quenching to various levels of undercooling below M_s (where M_s applies to the austenite present prior to quenching).

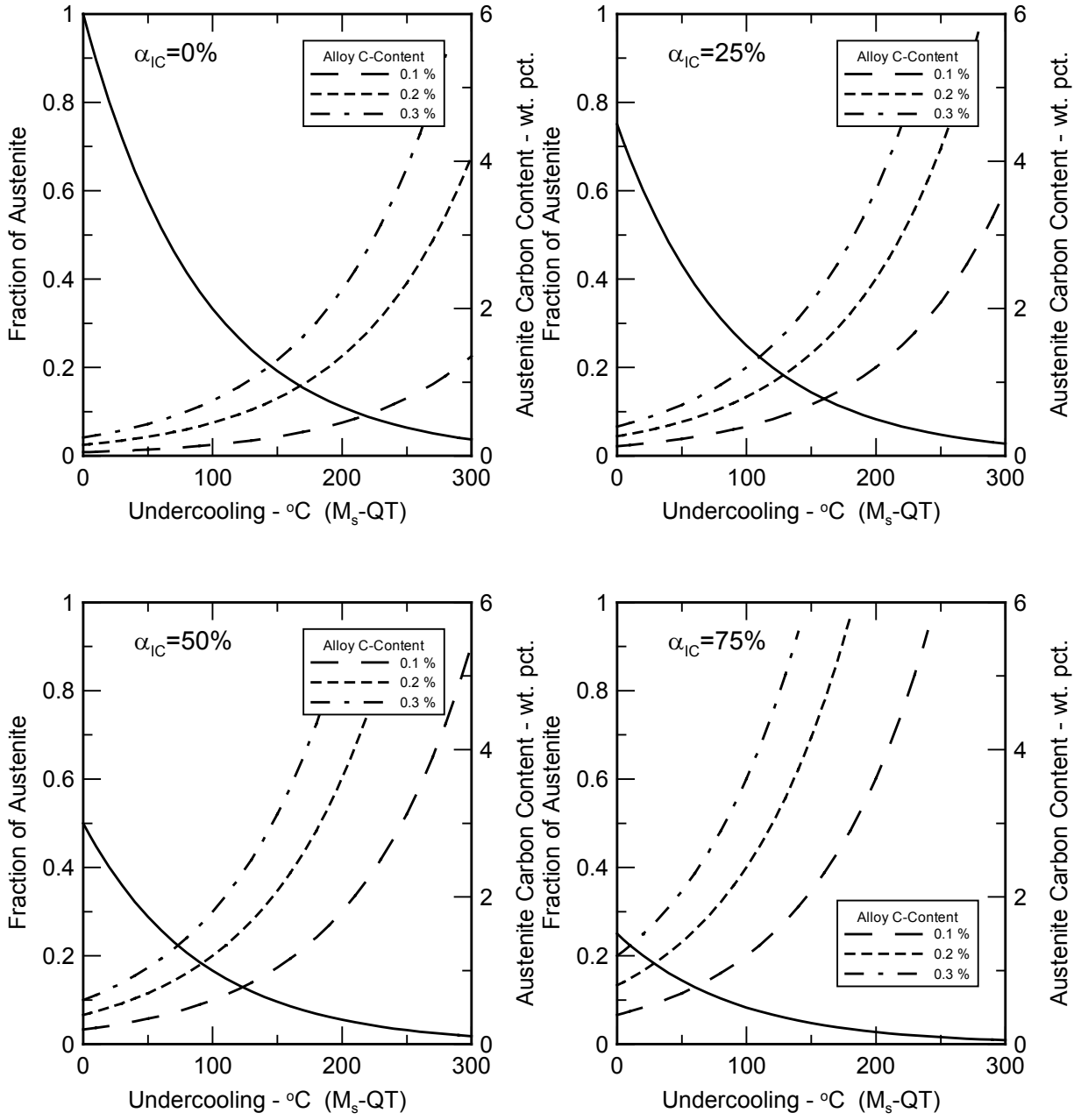

Figure 3. Calculated combinations of austenite fraction (solid lines) and austenite carbon concentrations (dashed lines) at the quench temperature (QT), plotted vs. undercooling below M_s for different fractions of intercritical ferrite and three different steel carbon levels.

The austenite fractions plotted in Figure 3 apply at the quench temperature, rather than after final cooling to room temperature. The four different graphs apply to four different initial annealing steps, including full austenitization where the amount of intercritical ferrite is zero, and treatments where the amount of ferrite after intercritical annealing (α_{IA}) is either 25%, 50%, or 75%. The results in Figure 3 should provide a useful tool to understand the austenite present after quenching and partitioning under a variety of conditions. It should be noted that the estimates in Figure 3 assume that all of the carbon partitions to the austenite, that carbide formation is precluded, and that the amount of martensite follows the Koistinen and Marburger relationship. Density differences between austenite and ferrite are also ignored for these

purposes whereby the weight and volume fractions of the phases are taken to be essentially identical.

The results in Figure 3 do not account for any reduction in the amount of austenite lost during final quenching after a partitioning treatment, although this behavior can also be predicted for a particular steel using the same concepts. The model was therefore extended to incorporate final cooling. An analysis was conducted for the experimental steel used in the present study, and the results are summarized in Figure 4 for a starting condition having 50% intercritical ferrite. In this figure, the *final* austenite fraction after partitioning and cooling to room temperature is plotted (bold solid line) vs. the quenching temperature prior to partitioning. The calculation essentially applies the Koistinen-Marburger relationship to the final quenching step to room temperature (~25^{o}C), using the austenite composition after full partitioning.

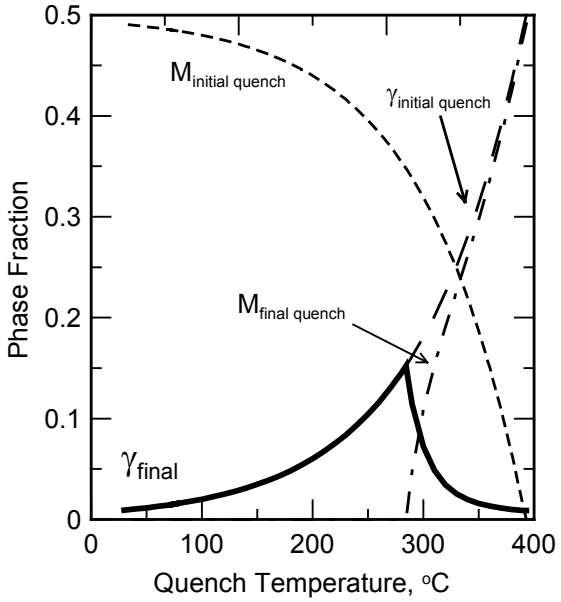

Figure 4. Predicted Q&P microstructure components for experimental steel containing 50% intercritical ferrite, vs. quench temperature, assuming full partitioning prior to final quenching to room temperature. The final austenite fraction at room temperature is given by the solid bold line. Dashed lines represent the austenite and martensite (M) present at the initial quench temperature, and the additional martensite formed during the final quench to room temperature. It should be noted that $\alpha_{IC} + M_{initial\ quench} + M_{final\ quench} + \gamma_{final} = 1$, and $\alpha_{IC} = .5$ in this example.

The results indicate an "optimum" quenching temperature that yields a maximum amount of retained austenite. The maximum austenite fraction is predicted to be about 15% in this steel, associated with a quench temperature of about 284^{o}C. This condition corresponds to the processing route identified for initial experimental investigation, i.e. annealing to create 50% intercritical ferrite, followed by quenching to 284^{o}C. The dashed curves in Figure 4 show key microstructural components, and help to explain the interesting relationship between the predicted final amount of retained austenite and the quench temperature. These microstructural components include the austenite and martensite present at the quench temperature after the initial quench, and the additional martensite that forms during the final quench to room temperature. Above the peak temperature, substantial austenite fractions remain after the initial quenching step, but the austenite stability is too low during final quenching, and increasing amounts of $M_{final\ quench}$ are found at higher quench temperatures, reducing the final austenite fraction at room temperature. Below the peak temperature too much austenite is consumed

during the initial quench prior to carbon partitioning, and the carbon content of the retained austenite is greater than needed for stabilization at room temperature. The peak is found at the particular quench temperature where martensite formation is just precluded during the final quench (i.e. where $M_{final\ quench}$ vanishes). This temperature corresponds to austenite having an M_s temperature of room temperature after full partitioning.

Similar calculations were made for the experimental steel, assuming variations in the intercritical ferrite fraction including 0% (full austenitization), 25%, 50%, and 75%. The final austenite fractions are plotted vs. quench temperature in Figure 5, except that a curve is not plotted for the condition representing 25% intercritical ferrite, because the final austenite fractions were almost indistinguishable from those of the fully austenitized condition. The results show that the maximum possible austenite fraction of about 15% in this steel can be achieved through different annealing routes which vary the fraction of intercritical ferrite, and correspondingly, perhaps the strength of the base microstructure.

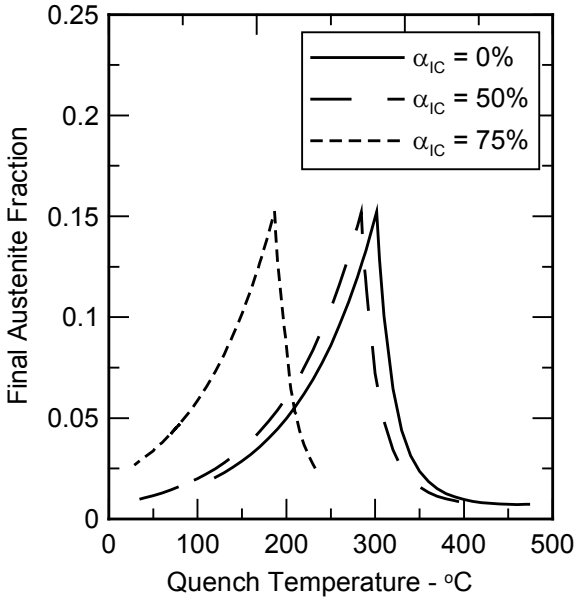

Figure 5. Calculated final austenite fraction after partitioning and cooling to room temperature for experimental steel, having 0, 50, or 75% intercritical ferrite.

It is also interesting to note that the positions of the curves imply that the quench temperature associated with the maximum austenite fraction should be somewhat less sensitive to intercritical annealing temperature at relatively low intercritical ferrite fractions. A higher carbon concentration in the alloy would be required to increase the maximum possible austenite fraction.

From a Q&P alloy and process design perspective, the methodology developed here is quite useful, and provides predictive capability for all of the key processing responses other than the partitioning *kinetics*. The calculations also indicate, not surprisingly, that the maximum possible retained austenite fraction is directly related to the total carbon content in the steel. Multistep heat treatment concepts can also be designed, to create microstructures with austenite regions having different carbon contents, although careful control of partitioning kinetic issues would also be required in such scenarios.

Experimental Verification

Procedures

Coupons (38.5 mm x 19.0 mm) nominally 1.0 mm in thickness were prepared for heat treating from a laboratory-produced sheet steel obtained in the cold rolled condition. Intercritical annealing was conducted in a molten salt bath for 180 s. Preliminary annealing and quenching studies showed that an intercritical annealing temperature of 805°C would provide the desired intercritical microstructure containing nearly equal fractions of ferrite and austenite, and this temperature was used for all of the treatments reported here. An example microstructure is shown in Figure 6 after intercritical annealing and water quenching; quantitative measurements indicate about 45 vol. % austenite and 55 vol. % ferrite. All Q&P samples were quenched from the intercritical temperature directly into a molten tin bath held at the desired QT value of 284°C and held for 3 s. The samples were then up-quenched into a molten salt bath to conduct the partitioning treatment at various times and temperatures, followed by subsequent water quenching to room temperature. Partitioning temperatures included 300, 350, 400, and 450°C, for times of 10, 100, and 1000 s at each temperature. After heat treatment, the austenite volume fractions and carbon contents were measured by x-ray diffraction.

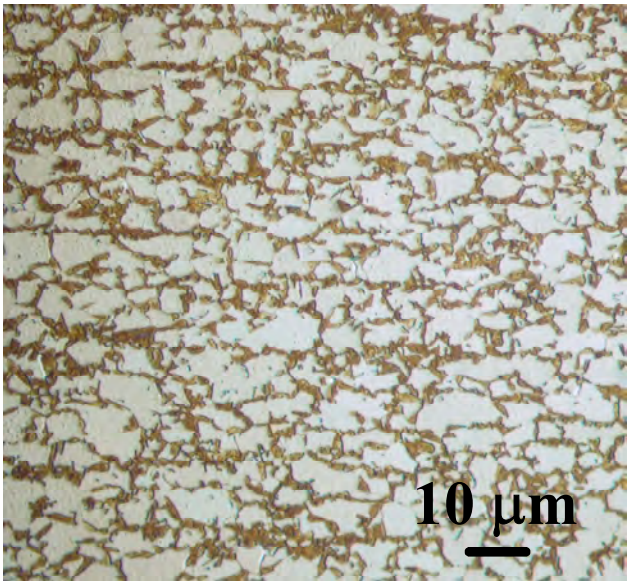

Figure 6. Microstructure of experimental steel after intercritical annealing 180 s at 805°C followed by water quenching. (Light optical)

The x-ray samples were chemically thinned to approximately 0.75 mm to remove effects of heat treating on near-surface microstructures, in a water-cooled beaker containing 50 ml of distilled water, 50 ml of 30% hydrogen peroxide, and 5 ml of hydrofluoric acid. Filtered copper radiation was used and eight diffraction peaks, including four austenite and four ferrite peaks, were monitored. Samples were scanned over a 2θ range from 40° to 105° using a step size of 0.02° and a dwell time of 2 s, using a Phillips X-pert diffractometer operating at 45kV and 40mA with a graphite monochromator. The integrated area and position of each peak was determined using the Phillips peak fitting software. A relationship incorporating the integrated intensities of the {111}, {200}, {220}, and {311} austenite peaks and the {110}, {200}, {211}, and {220} ferrite peaks in addition to R-values for each peak was used to quantify austenite volume fraction for the TRIP steel used in this study [20]. This approach is reported to account well for possible texture effects, since numerous austenite and ferrite peaks are included in the calculation [20]. R-values are a function of θ (degrees), hkl, and the crystal structure and composition of each phase, and are representative of calculated theoretical intensity values

[20,21]. The R-values used in retained austenite determination for this study were obtained using unit cell volumes calculated from experimentally measured lattice parameters, which inherently incorporate the carbon and alloy content [21]. Ferrite and martensite were both treated as body centered cubic for these calculations. Additionally, when $K_{\alpha 1}$ and $K_{\alpha 2}$ peaks were present for ferrite, the integrated intensity incorporated only the $K_{\alpha 1}$ peak. Associated calculations used the $K_{\alpha 1}$ wavelength. When $K_{\alpha 1}$ and $K_{\alpha 2}$ were not distinguishable and a single peak was present, the $K_{\alpha\ wtd.}$ wavelength (a weighted average) was used. The Lorentz-polarization factor was modified to account for the use of a graphite monochromator.
Austenite carbon content was calculated using the expression [21]:

$$a_0 = 3.555 + 0.044x \tag{7}$$

where a_0 is austenite lattice parameter in Angstroms and x is carbon content in weight percent. The lattice parameter was estimated from an average based on the {220} and {311} austenite peaks, since peak position could be most accurately determined for these high angle peaks.

Microstructures were evaluated with light and SEM metallographic techniques using polished and etched samples. The light microscopy samples used a two-step picral / sodium metabisulfite tint-etching procedure [22], while the SEM samples were etched in 2% nital.

Results and Discussion

Following the processing plan designed with the methodology discussed above, the initial experimentation reported here involved intercritical annealing to form ferrite and austenite, quenching to 284°C (the temperature where about 15% austenite was expected), and then examining the partitioning response at various times/temperatures. The volume fraction of austenite retained at room temperature, and the carbon content of the retained austenite are the critical results.

The retained austenite fractions after intercritical annealing at 805°C, quenching to 284°C, then up-quenching and partitioning at temperatures between 300°C and 450°C, followed by water cooling to room temperature, are plotted vs. partitioning time in Figure 7. The associated chemical compositions of the retained austenite are plotted in Figure 8 vs. partitioning temperature. If the samples were quenched directly to room temperature from the intercritical annealing temperature, it should be noted that there was *no* retained austenite detected in the x-ray diffraction patterns. This behavior is represented by extrapolation of the short-time partitioning data in Figure 7, and indicates that the partitioning treatment is *required* for any austenite to be stabilized to room temperature after quenching. The austenite fraction and composition are both reflective of the partitioning kinetics represented in Figures 7 and 8. The final fraction of retained austenite generally increases with partitioning time, and increases faster at higher temperature, as expected for a carbon diffusion controlled process.

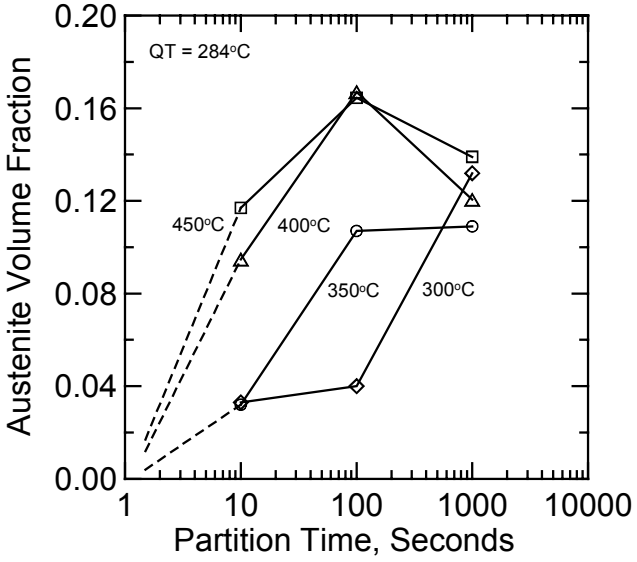

Figure 7. Final austenite fraction at room temperature in an experimental high-Al TRIP steel after various partitioning treatments (QT=284°C).

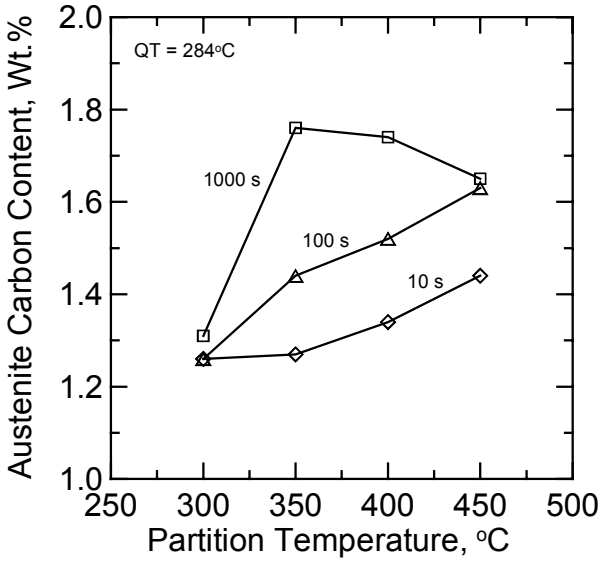

Figure 8. Measured carbon concentration of retained austenite in an experimental high-Al TRIP steel after various partitioning treatments (QT=284°C).

At the higher temperatures, the retained austenite fraction decreases slightly at the longest partitioning time of 1000 s. This behavior may be due to the onset of carbide precipitation (possibly in combination with some bainite formation) that would consume some of the available carbon, although no carbide peaks were yet evident in the x-ray diffraction patterns. At the lowest temperature, 300°C, the amount of retained austenite was still increasing at the longest partitioning time investigated. It is especially noteworthy that substantial fractions of retained austenite were found in these samples, exceeding the aim 15% in some instances. The Q&P process is thus considered to be capable of producing quite encouraging results. Furthermore, the peak in retained austenite fraction may not yet have been identified for this steel, since only three partitioning times were examined at each temperature.

The carbon concentration of the austenite is seen to increase with aging temperature in Figure 8, and the overall trend is to reach higher levels with increased partitioning time. These behaviors

are consistent with carbon diffusion controlled processes. An example of the change in the x-ray diffraction spectrum with partitioning time at 400°C is shown in Figure 9, using the $\{111\}_{austenite}$ and $\{110\}_{ferrite}$ peaks. After intercritical annealing and water quenching, the austenite peak is not evident, and broadening of the ferrite peak is suggestive of a "shoulder" associated with tetragonal as-quenched martensite. After a 10 s partitioning treatment and then cooling to room temperature, the martensite shoulder is diminished, and the austenite peak becomes visible, suggestive of carbon partitioning between martensite and austenite. At longer partitioning time, the austenite peak increases in intensity, and decreases in 2θ, indicating an increase in austenite fraction and an increase in lattice parameter associated with increased carbon enrichment. A small decrease in carbon content is apparent in Figure 8 at higher temperatures at the longest partitioning time, possibly associated with the onset of carbide formation, although carbide peaks were not yet present in the diffraction results. The combinations of austenite fraction and carbon content measured here are attractive, and in some instances exceed what could be expected from full partitioning in a steel containing 0.19% carbon. This discrepancy is likely a result of some inaccuracies in the x-ray results, such as fitting of low intensity peaks, or residual stress effects that may influence the peak positions along with the solute carbon levels.

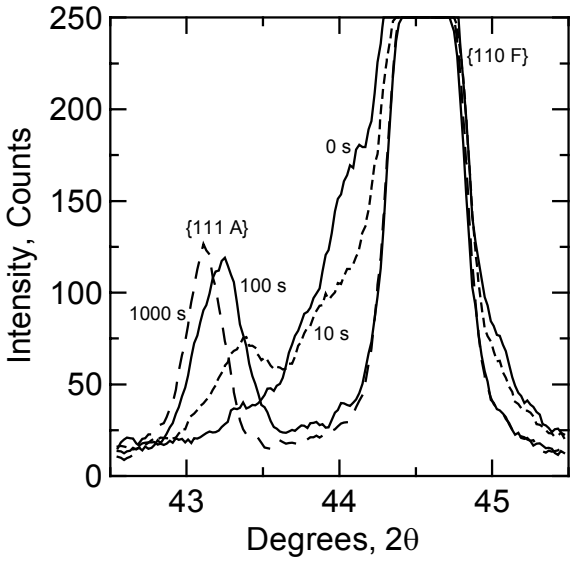

Figure 9. X-ray spectra illustrating changes in the $\{111\}_\gamma$ and $\{110\}_\alpha$ peaks during partitioning at 400°C in experimental steel intercritically annealed at 805°C and quenched to 284°C.

Microstructural studies on the Q&P sheet specimens are currently underway. Figure 10 shows an example microstructure, obtained using the SEM for the sample given a 100 s partitioning treatment at 400°C. The micrograph shows dark featureless intercritical ferrite, with a blocky martensite-austenite (or retained austenite) constituent, and finer lath-like features that appear quite similar to the carbide-free bainite plus retained austenite morphology observed in conventional TRIP sheet steels (shown by arrow). It is not clear yet whether these features are the result of a process involving transformation to martensite followed by partitioning of carbon into the untransformed austenite, or a more conventional bainitic ferrite growth mechanism that may

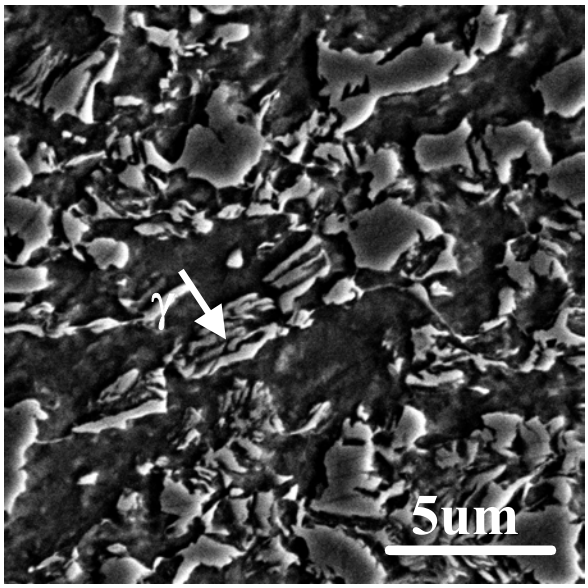

Figure 10. Microstructure of experimental steel after intercritical annealing (50%γ) followed by quenching to 284°C and partitioning 100 s at 400°C. (SEM)

compete with the proposed Q&P mechanisms in any pools of austenite that are untransformed at the quench temperature. The quantitative predictions made in the Q&P process design section above are especially sensitive to the accuracy of M_s temperature of the austenite. Consequently, experimental verification of the M_s temperature and the martensite volume fraction present at the quench temperature would be helpful in this high-Al steel, along with in-depth microstructure characterization. However, it should be noted that substantial fractions of carbon enriched austenite have also been found recently in Q&P specimens of this steel processed with a lower quench temperature of 234°C. It is much less likely that sufficient (untransformed) austenite remained at this quench temperature for bainite growth into this austenite to have been capable of providing and alternative mechanism for obtaining the austenite fractions retained at room temperature.

Conclusions

1. The constrained paraequilibrium model for carbon partitioning between quenched martensite and retained austenite is reviewed. While rigorous calculations may be made to determine the conditions where the chemical potential of carbon is equal in the ferrite and austenite, subject to the matter balance constraint associated with a stationary α/γ interface during partitioning, the austenite composition at constrained paraequilibrium may be reasonably approximated by assuming that virtually all of the carbon in the martensite partitions to austenite.
2. Further studies are needed to understand the influences of alloying and processing (time/temperature) on the onset of transition carbide precipitation, which may be undesired during the partitioning treatment associated with Q&P. In the meantime, avoidance of very low partitioning temperatures might be expected to mitigate formation of transition carbides.
3. A simple model is presented to predict the microstructure response to quenching and partitioning heat treatments, assuming full partitioning of carbon into austenite. The model is useful for process design, and indicates an optimum quenching temperature to

maximize the amount of austenite retained at room temperature. The maximum austenite fraction is hypothesized to correspond with carbon enrichment to a level where the M_s temperature of the austenite after partitioning corresponds to room temperature.

4. Initial experimental results on a 0.19C, 1.46Mn, 1.96Al sheet steel verify that substantial amounts of carbon-enriched austenite can be obtained through Q&P processing, with measured retained austenite fractions similar to the aim maximum of 15% in this steel. The partitioning kinetics are also characterized at temperatures between 300 and 450^{o}C and partitioning times of 10 100, or 1000 s in samples processed with 50% intercritical ferrite, and generally indicate greater increases in retained austenite fraction and austenite carbon content with higher temperatures and longer times. Decreasing austenite carbon enrichment at longer times at the highest temperature may be associated with the onset of carbide precipitation (possibly in combination with some bainite formation), although carbide peaks were not yet observed in the x-ray diffraction spectra.
5. The microstructure of the experimental high-Al steel after intercritical annealing, quenching, and partitioning at 400^{o}C consists of intercritical ferrite with a blocky martensite-austenite or retained austenite constituent, and finer lath-like features that appear quite similar to carbide-free bainite mixtures of ferrite and retained austenite. Clarification of the transformation behavior will be aided by confirmation of the predicted M_s temperatures, and further microstructural characterization at resolutions greater than available in the SEM.

Acknowledgements

The authors gratefully acknowledge the support of the Advanced Steel Processing and Products Research Center, a National Science Foundation Industry/University Cooperative Research Center at the Colorado School of Mines, and the Inter-American Materials Collaboration Program of the NSF (USA) and CNPq (Brazil). Ispat-Inland Steel Company is gratefully acknowledged for providing the experimental steel and its associated chemical composition.

References

1. H.K.D.H. Bhadeshia, *Bainite in Steels*, (London: The Institute of Materials, 2001).
2. J.G. Speer, D.K. Matlock, B.C. De Cooman, and J.G. Schroth, "Carbon Partitioning into Austenite After Martensite Transformation," *Acta Materialia*, 51 (2003), 2611-2622.
3. D.K. Matlock, V.E. Bräutigam, and J.G. Speer, "Application of the Quenching and Partitioning (Q&P) Process to a Medium-Carbon, High-Si Microalloyed Bar Steel", *Proceedings of THERMEC' 2003*, (Uetikon-Zurich, Switzerland: Trans. Tech. Publications, Inc., 2003), 1089-1094.
4. A. Hultgren, "Isothermal Transformation of Austenite", *ASM Transactions*, 39 (1947), 915-1005.
5. J.A. Lobo and G.H. Geiger, "Thermodynamics and Solubility of Carbon in Ferrite and Ferritic Fe-Mo Alloys," *Metallurgical Transactions A*, 7A (1976), 1347-1357.
6. J.A. Lobo and G.H. Geiger, "Thermodynamics of Carbon in Austenite and Fe-Mo Austenite," *Metallurgical Transactions A*, 7A (1976), 1359-1364.
7. M. Hillert, L. Hoglund, and J. Agren, "Escape of Carbon from Ferrite Plates in Austenite," *Acta Metallurgica et Materialia*, 41 (1993), 1951-1957.
8. H.K.D.H. Bhadeshia and D.V. Edmonds, "The Bainite Transformation in a Silicon Steel," *Metallurgical Transactions A*, 10A (1979), 895-907.
9. M.F. Gallagher, J.G. Speer, D.K. Matlock, and N.M. Fonstein, "Microstructure Development in TRIP-Sheet Steels Containing Si, Al, and P," *Proceedings of the 44th*

Mechanical Working and Steel Processing Conference, (Warrendale, PA: Iron and Steel Society, 2002), 153-172.
10. G. Krauss, *STEELS: Heat Treatment and Processing Principles*, (Metals Park, OH: ASM International, 1990).
11. R.W.K. Honeycombe and H.K.D.H. Bhadeshia, *Steels, Microstructure and Properties*, (London: Edward Arnold, 1995).
12. G. Krauss, "Tempering and Structural Change in Ferrous Martensitic Structures," *Proceedings of an International Conference on Phase Transformations in Ferrous Alloys*, (Warrendale,PA: The Metallurgical Society of AIME, 1984), 101-123.
13. H-C Lee and G. Krauss, "Intralath Carbide Transitions in Martensitic Medium-Carbon Steels Tempered Between 200 and 300^{o}C," *Gilbert R. Speich Symposium Proceedings: Fundamentals of Aging and Tempering in Bainitic and Martensitic Steel Products*, (Warrendale, PA: Iron and Steel Society, 1992), 39-43.
14. L. L. Barbe, B.C. De Cooman, and K. Conlon, "Characterization of the Metastable Austenite in Low-alloy Fe-C-Mn-Si TRIP-aided Steel by Neutron Diffraction," *Zeitschrift fur Metallkunde*, 93 (2002), 1217-1227.
15. T.N. Rouns and K.B. Rundman, "Constitution of Austempered Ductile Iron and Kinetics of Austempering", *AFS Transactions*, 95 (1987), 851-874.
16. L. Sidjanin, R.E. Smallman, and J.M. Young, "Electron Microstructure and Mechanical Properties of Silicon and Aluminium Ductile Irons", *Acta Metallurgica et Materialia*, 42 (1994), 3149-3155.
17. R. Le Houillier, G. Bégin, and A. Dubé, "A Study of the Peculiarities of Austenite During the Formation of Bainite," *Metallurgical Transactions*, 2 (1971), 2645-2653.
18. M.F. Gallagher, J.G. Speer, and D. K. Matlock, "Effect of Annealing Temperature on Austenite Decomposition in a Si-Alloyed TRIP Steel," *Austenite Formation and Decomposition*, ed. E.B. Damm and M. Merwin (Warrendale, PA: ISS/TMS, 2003).
19. M. De Meyer, J. Mahieu, and B.C. De Cooman, "Empirical Microstructure Prediction Method for Combined Intercritical Annealing and Bainitic Transformation of TRIP Steel," *Materials Science and Technology*, 18 (2002), 1121-1132.
20. *Retained Austenite and Its Measurement by X-Ray Diffraction, SP-453*, (Warrendale, PA: Society of Automotive Engineers, Inc., January 1980), 12.
21. B.D. Cullity, *Elements of X-Ray Diffraction*, 2nd Ed., (Addison-Wesley Publishing Co., Inc., 1978).
22. A.K. De, J.G. Speer, and D.K. Matlock, "Color Tint-Etching for Multiphase Steels," *Advanced Materials and Processes*, 161 (February 2003), 27-30.